AN EXPERIMENTAL INVESTIGATION OF THE SEPARATING/REATTACHING FLOW OVER A BACKSTEP

Progress Research Report

Cooperative Agreement No.: NCC2-465

for the period

January 1, 1991 - August 31, 1991

Submitted to

National Aeronautics and Space Administration
Ames Research Center
Moffett Field, California 94035

Experimental Fluid Dynamics Branch
Joseph G. Marvin, Chief
David M. Driver, Technical Monitor

Fluid Dynamics Division
Paul Kutler, Chief

Prepared by

ELORET INSTITUTE
1178 Maraschino Drive
Sunnyvale, CA 94087
Phone: 408-730-8422 and 415-493-4710
Telefax: 408-730-1441
K. Heinemann, President and Grant Administrator
Srboljub Jovic, Principal Investigator

10 December, 1991

INTRODUCTION

This progress report covers the grant period from January until the end of August 1991.

Reynolds number effencts on the evolution of the turbulence structure in the recovery region of a turbulent separated flow generated by a backward-facing step were studied experimentally. Five different flow conditions and four Reynolds numbers were investigated. All single-point measurements were conducted on the plane of symmetry of the wind tunnel starting at approximately $x/h = 10$ for each flow condition. The upper limit of the measuring domain depends upon the physical size of the tunnel and ranged from 50 to 114 step heights. It is apparent that the most of the boundary layer recovery was captured by the experiment. Normal stresses, shear stress, mixing length scales and eddy viscosity are shown in this progress report while the higher order velocity products related to the diffusion of the turbulence energy are planned for latter stages of the data analysis.

EXPERIMENTAL CONDITIONS AND TECHNIQUES

The experiments were conducted in the same tunnel as described in the previous progress reports. This is a 200 x 400 mm low-speed suction-type wind tunnel with a 4.0m long test section. The recovery of the boundary layer was investigated for five different flow conditions or four Reynolds numbers with one Reynolds ($R_h = 25500$) number being obtained by the two different combination of U_{ref} and h.

Initial condition

Reynolds number based on the step height, h, and the reference velocity, U_{ref}, upstream of the step ranged from 6800 to 37000. Experiments were conducted for five different combinations of the reference velocity, U_{ref}, and the step height, h, which are given in the table bellow.

Table 1. Flow conditions

R_h	$U_{ref}(m/s)$	$h(mm)$
6800	6.0	17
10500	6.0	26
25500	14.7	26
25500	10.0	38
37000	14.7	38

The boundary layer upstream of the step was turbulent and fully developed such that the incoming boundary layer thickness was approximately constant in all five cases.

Experimental Technique

Direct measurements of the skin friction coefficient were obtained using the Laser-oil interferometry technique. . A normal hot-wire probe was used to measure the of a streamwise velocity flictuations, u', very close to the wall.. In some streamwise locations the first measuring point was as low as one wall unit. A cross hot wire probe was used to measure $\overline{u^2}$, $\overline{v^2}$ and $\overline{uv}$. The first point for these measurements was about $y^+ = 20$ wall units.

RESULTS AND DISCUSSION

Skin friction coefficient distributions for different Reynolds numbers are shown in Figure 1. Negative values of skin friction in the recirculating zone reduce as the Reynolds number, R_h increases. In the recovery region, skin friction asymptotically approache distribution for highest value of Reynolds number. Mean velocity profiles normalized by the measured friction velocity, u_τ, for $R_h = 25500$ are shown in Figure 2. It is apparent that the law of the wall is violated sufficiently close to the mean reattachment point reflecting nonequilibrium nature of the flow in this region. Further downstream, for $x/h \geq 30$, mean velocity profiles correlate well with the standard law-of-the-wall distribution in the near wall region. This suggests that the near-wall turbulence structure may resemble that found in a regular equilibrium boundary layer. This notion is further confirmed by the fact that the distributions of u_{rms}/u_τ, v_{rms}/u_τ and $-\overline{uv}/u_\tau^2$ (see Figure 3. for $R_h = 25500$) agree well with Klabanoff's measurements in the near wall region. It appears that the near-wall structure recovered by the distance of $30h$ downstream from the step. Note should be made that the Reynolds numbers of the two experiments were comparable. The Reynolds numbers based on the momentum thickness of the Klebanoff and the present experiment were 7500 and about 7000 respectively.

The turbulence structure of the outer flow region reflected by u_{rms}/u_τ, v_{rms}/u_τ and $-\overline{uv}/u_\tau^2$ approaches the structure of an equilibrium boundary layer at a much slower rate than near the wall. The Reynolds shear stress is shown in Figure 4 for the tested Reynolds number range. Higher energy content, present in the wake region for all Reynolds numbers, is due to the presence of the large coherent structures convected downstream from their origin in the free shear layer region. The rate of the brake-down of these structures and their approach to that found in a regular equilibrium turbulent boundary layer depends on the intensity of the perturbation imposed by the step. The intensity of a perturbation is generally a function of R_h, δ/h, E_r (expansion ratio) and the state of the upstream boundary layer (turbulent or laminar). In this experiment the expansion ratio, E_r, varied from 1.1 for $R_h = 6800$ to 1.2 for $R_h = 37000$, therefore it is safe to say that the adverse pressure gradient due to the different expansion ratios did not play an important role in flow dynamics. Pressure coefficient measurements for the different Reynolds numbers are planned for the next phase of the project. In all cases the incoming boundary layer was a fully developed turbulent boundary layer with approximately constant boundary layer thickness, $\delta = 30$ to $34mm$. Hence, the parameter δ/h changed only due to the variation of the step height and it varied between 0.8 and 2. According to Bradshaw & Wong (1972) the strength of perturbation for δ/h in the given range can be regarded as a strong to weak perturbation.

Turbulence mixing length scale, l/δ, distributions (Figure 5.) obtained from the mean velocity and the shear stress distributions indicate a presence of structures in the outer region with much larger length scales than those found in a regular boundary layer. The slope of the l/δ distribution near the wall and close to the reattachment zone is much greater from the value of $\kappa = 0.41$, where κ is von Kármán's constant. The slope monotonically approaches the above value of 0.41 for greater downstream distances. It appears that a more intense perturbation is created for a greater R_h when the parameter δ/h is kept constant (see Figure 5(b) and 5(c), for $R_h = 10500$ and $R_h = 25500$). Consistently, eddy viscosity distributions, $\nu/U_e\delta^*$ vs. y/δ (see Figure 6, δ^* is the displacement thickness), which were obtained from the measured shear stress and mean velocity distributions for different R_h, indicate more intense mixing of the flow than in a regular turbulent boundry layer. Neither the outer layer mixing length scale nor the eddy viscosity distribution does not approach those found in an equilibrium boundary layer even at $x/h = 114$ (see Figure 5(a) and 6(a) for $R_h = 6800$). This behavor shows that the transport of momentum due to turbulence, which is contained in triple velocity products or diffusion terms, still has a memory of perturbation experienced by the flow in the separated region. Additional analysis of triple products of velocity fluctuations will be presented in the next progress report.

FUTURE PLANS

The experiment in a recovery region of the separated flow indicated that the flow has not reached the equilibrium boundary layer structure even after $x/h \geq 100$ downstream of the step. While the turbulence structure approaches the regular boundary layer structure near the wall downstream of the step, the outer region structure remain dominated by large structures advected downstream from the free shear layer region.

It is expected from the two-point measurements made at $x/h = 38$ that the multipoint measurements of a velocity field can give very fruitful results. Hence, an objective of the future study is to analyze simultaneous velocity field using a rake of seven X-wires to investigate the evolving turbulence structure of the separated flow. These measurements will be performed for $R_h = 25500$ and possibly for one smaller Reynolds number.

ACKNOWLEDGMENT

The author is indebted to J. Marvin and D. Driver for their continuous encouragement throughout the experiment.

References

Head, M.R. and Bandyopadhyay, P. 1981 New Aspects of Turbulent Boundary- layer structure. *J. Fluid Mech.* **107**, 297.

Bradshaw, P. and Wong, F.Y.F., 1971, The Reattachment and Relaxation of a Turbulent Shear Layer. *J. Fluid Mech.* **52**, 113.

Jovic, S. and Browne, L.W.B. 1990 Turbulent Heat Transfer Mechanism in a Recovery Region of a Separated Flow. *Engineering Turbulence Modelling and Experiments Proceedings of the International Symposium on Engineering Turbulence Modeling and Measurements,* September 24-28, ed. W. Rodi and E.N. Ganic.

Moin, P. and Moser, R.D. 1989 Characteristic-eddy decomposition of turbulence in a channel.*J. Fluid Mech.* **200**, 471.

Theodorsen, T. 1952 Mechanism of Turbulence. In Proc. *2nd Midwestern Conf. on Fluid Mech.*, Ohio State University, Columbus, Ohio.

Townsend, A.A. 1976 *The Structure of the Turbulent Shear Flow.* Cambridge University Press.

Figure Captions

Figure 1. Skin friction distribution for different Reynolds numbers.

Figure 2. Mean velocity profiles in wall coordinates for $R_h = 25500$.

Figure 3. Reynolds stress profiles for $R_h = 25500$. (a) u_{rms}/u_τ; (b) v_{rms}/u_τ; (c) $-\overline{uv}/u_\tau^2$.

Figure 4. Shear stress profiles for different Reynolds numbers R_h: (a) 6800; (b) 10500; (c) 25500; (d) 25500; (e) 37000.

Figure 5. Mixing length scale distribution for different Reynolds numbers R_h: (a) 6800; (b) 10500; (c) 25500; (d) 25500; (e) 37000.

Figure 6. Eddy viscosity distributions for different Reynolds numbers R_h: (a) 6800; (b) 10500; (c) 25500; (d) 25500; (e) 37000.

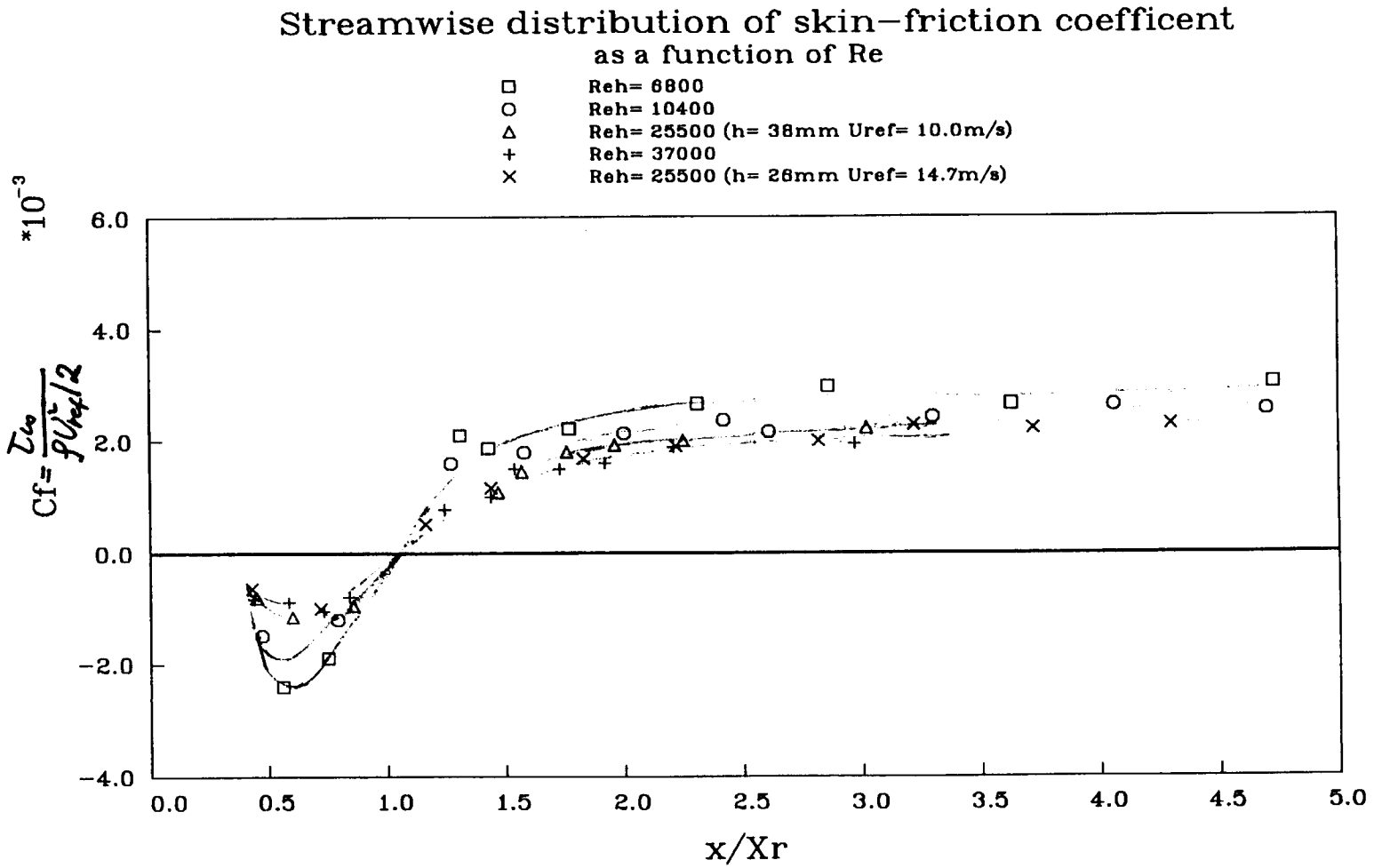
Streamwise distribution of skin−friction coefficent
as a function of Re
Reh= 6800
Reh= 10400
Reh= 25500 (h= 38mm Uref= 10.0m/s)
Reh= 37000
Reh= 25500 (h= 26mm Uref= 14.7m/s)
*10^-3
Cf= τw / ρUref^2/2
6.0
4.0
2.0
0.0
−2.0
−4.0
0.0
0.5
1.0
1.5
2.0
2.5
3.0
3.5
4.0
4.5
5.0
x/Xr

Figure 4.

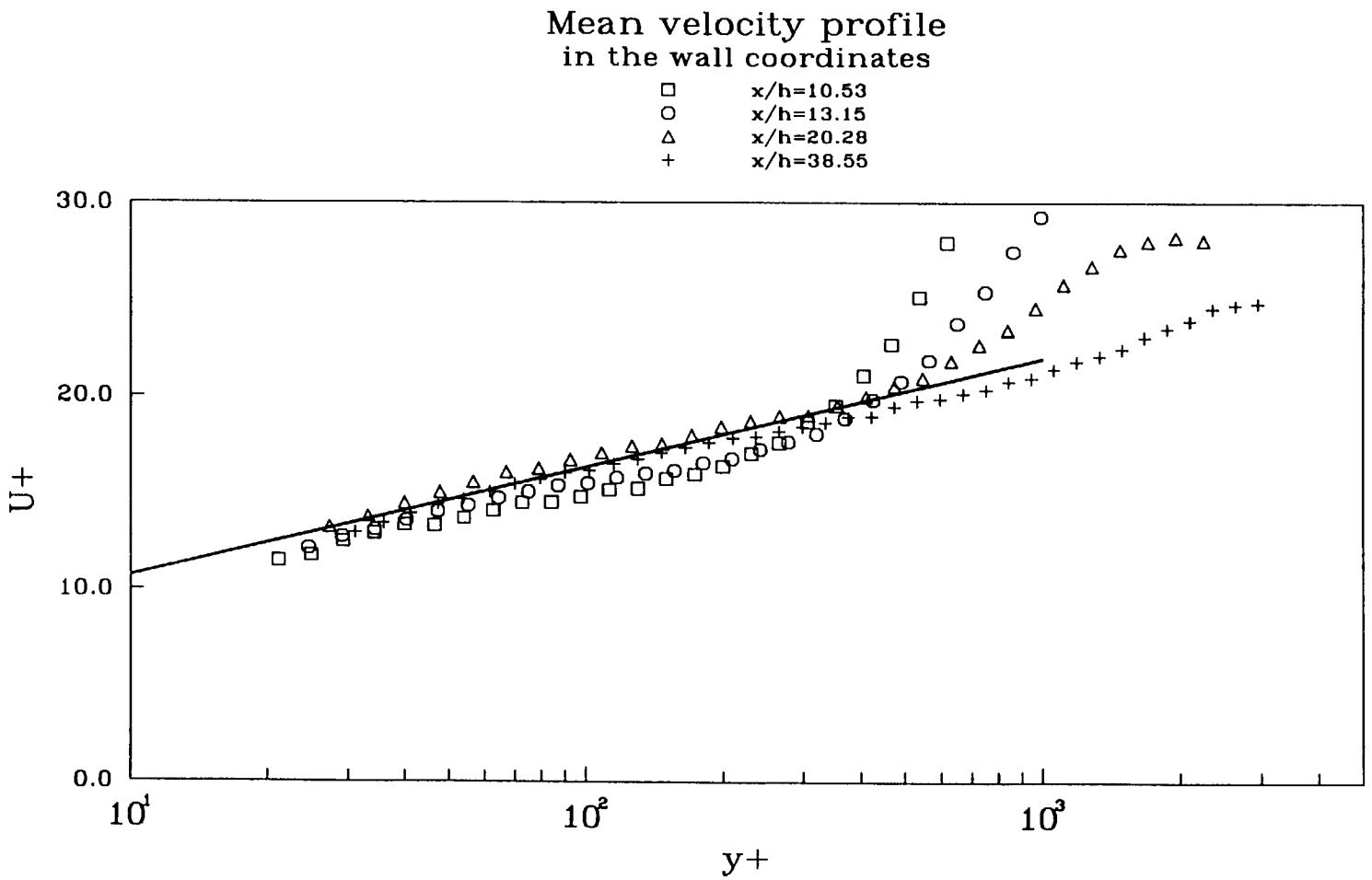
Mean velocity profile
in the wall coordinates
x/h=10.53
x/h=13.15
x/h=20.28
x/h=38.55
30.0
20.0
10.0
0.0
U+
10^1
10^2
10^3
y+

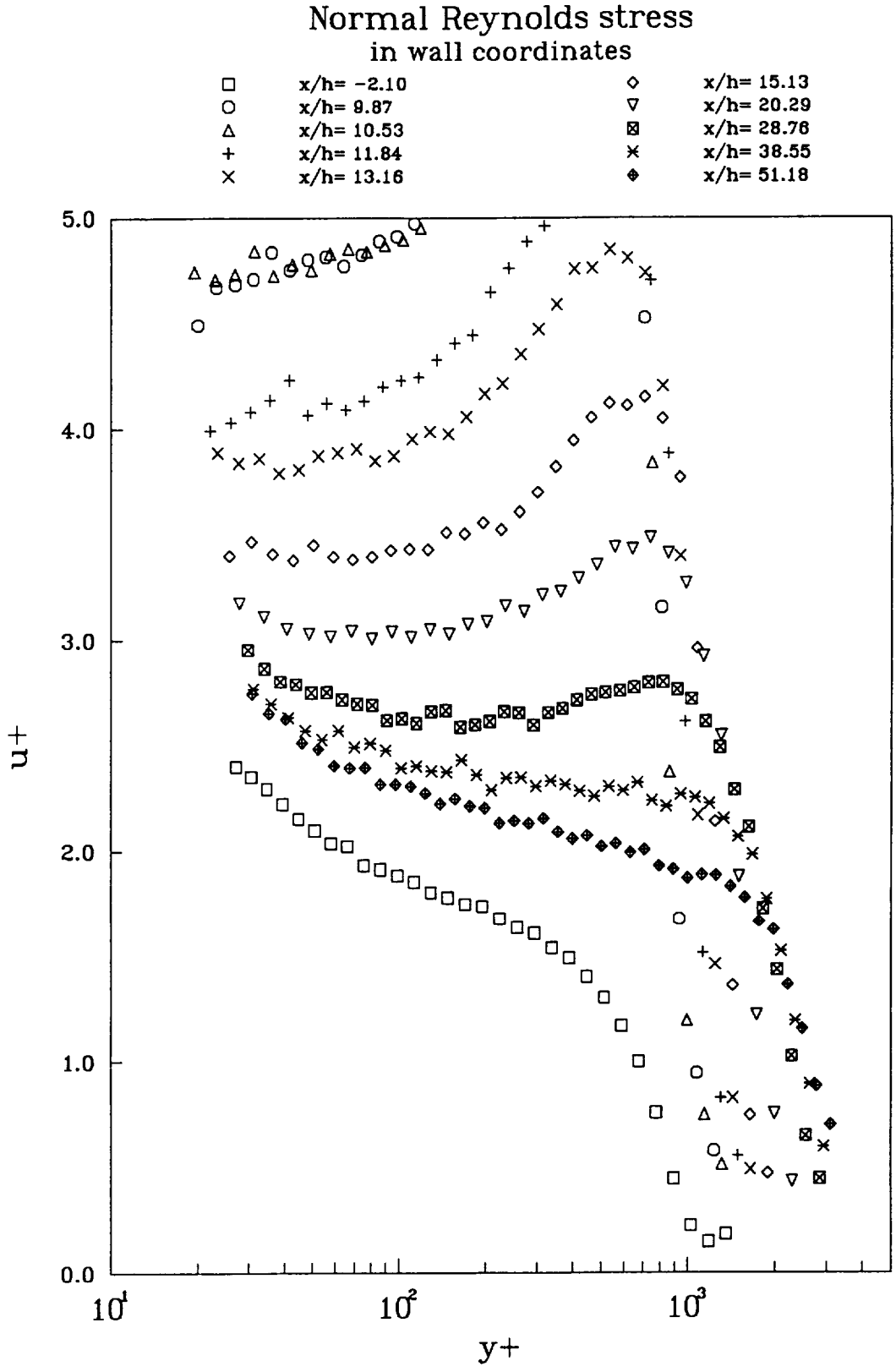
Normal Reynolds stress
in wall coordinates
x/h= -2.10
x/h= 9.87
x/h= 10.53
x/h= 11.84
x/h= 13.16
x/h= 15.13
x/h= 20.29
x/h= 28.76
x/h= 38.55
x/h= 51.18
5.0
4.0
3.0
2.0
1.0
0.0
u+
10^1
10^2
10^3
y+

Figure 2. (a)

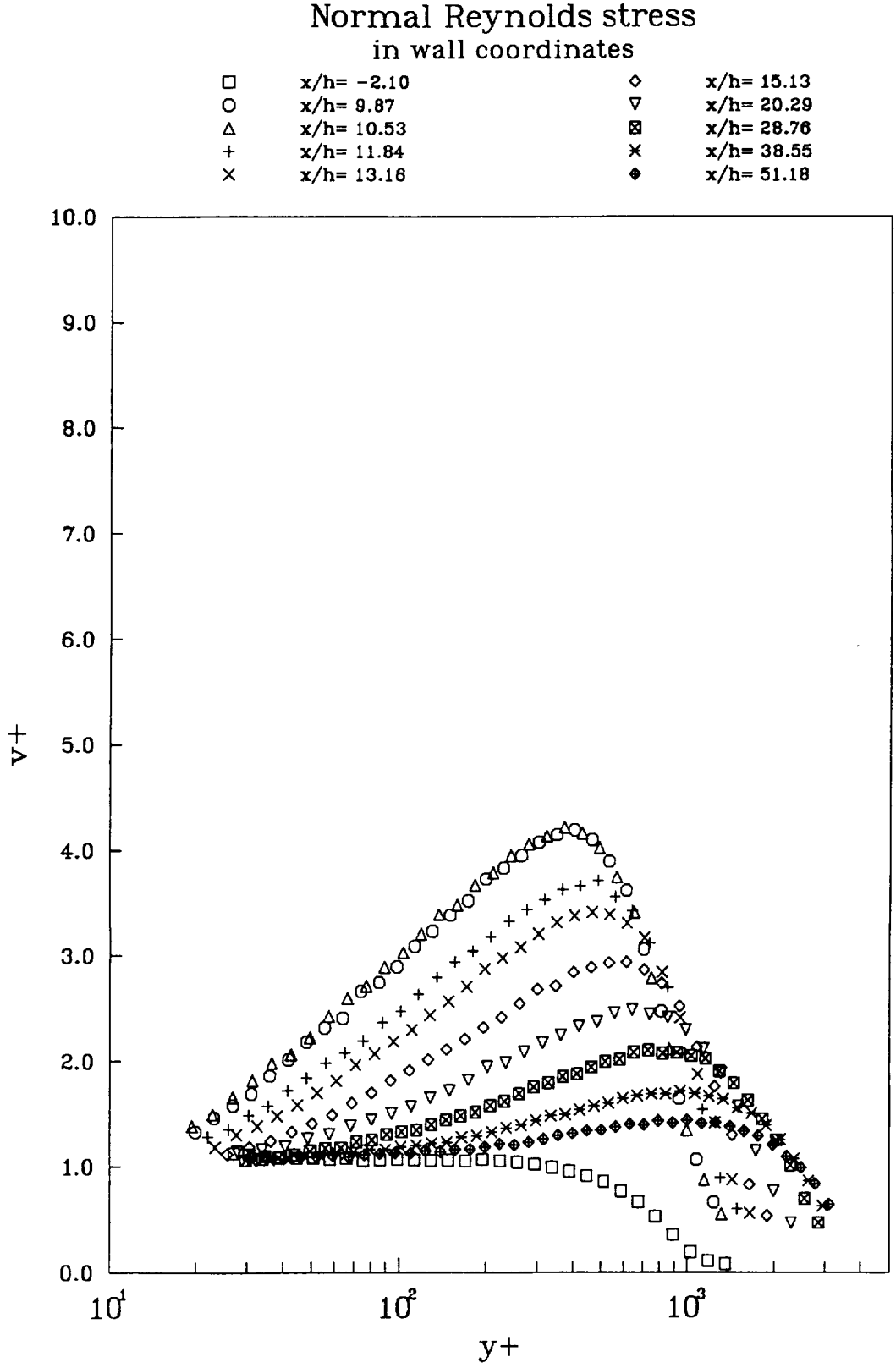
Normal Reynolds stress
in wall coordinates
x/h= -2.10
x/h= 9.87
x/h= 10.53
x/h= 11.84
x/h= 13.16
x/h= 15.13
x/h= 20.29
x/h= 28.76
x/h= 38.55
x/h= 51.18
10.0
9.0
8.0
7.0
6.0
5.0
4.0
3.0
2.0
1.0
0.0
v+
10^1
10^2
10^3
y+

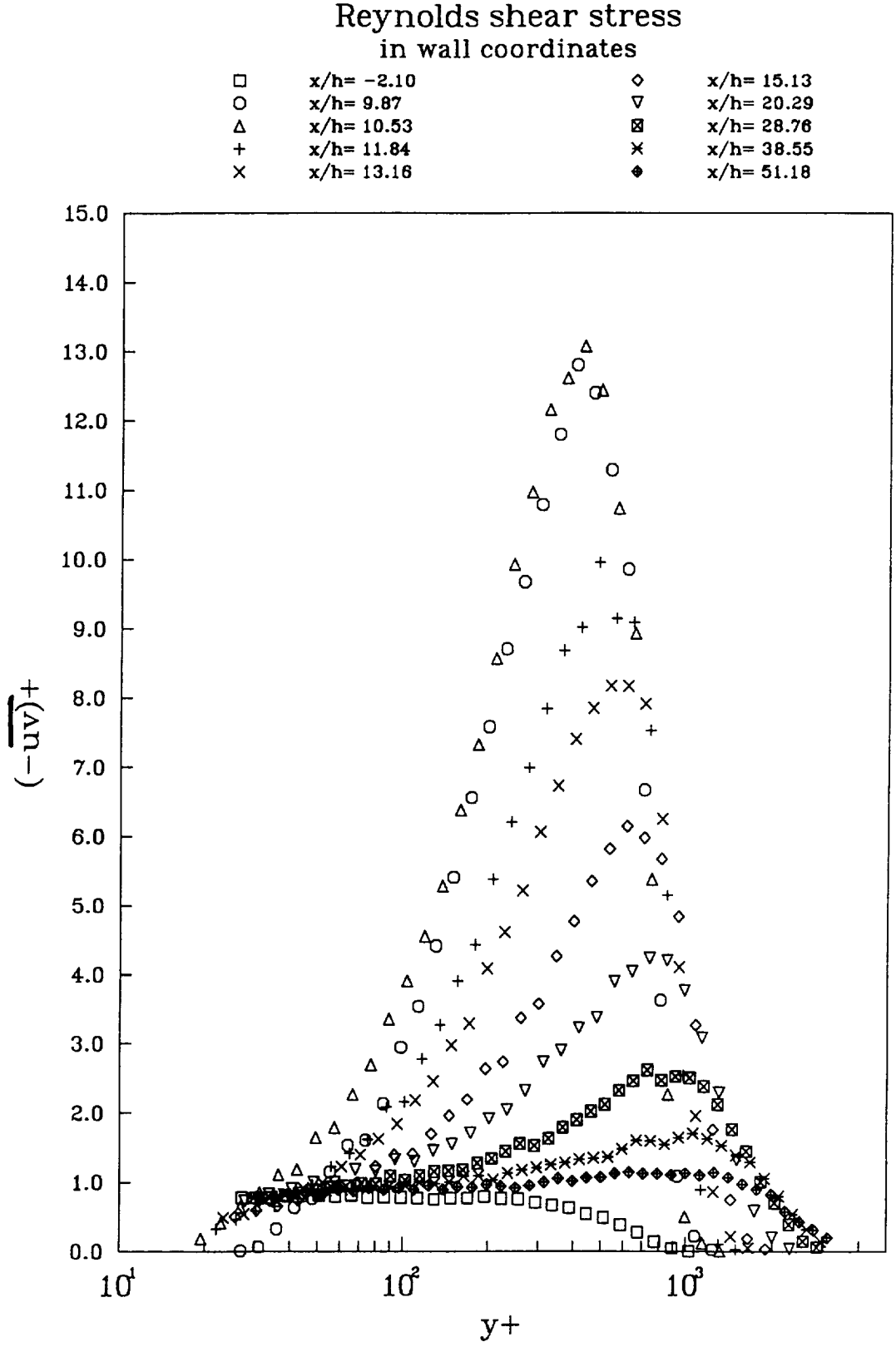
Reynolds shear stress
in wall coordinates
x/h= -2.10
x/h= 9.87
x/h= 10.53
x/h= 11.84
x/h= 13.16
x/h= 15.13
x/h= 20.29
x/h= 28.76
x/h= 38.55
x/h= 51.18
15.0
14.0
13.0
12.0
11.0
10.0
9.0
8.0
7.0
6.0
5.0
4.0
3.0
2.0
1.0
0.0
$\overline{(-uv)}+$
10^1
10^2
10^3
y+

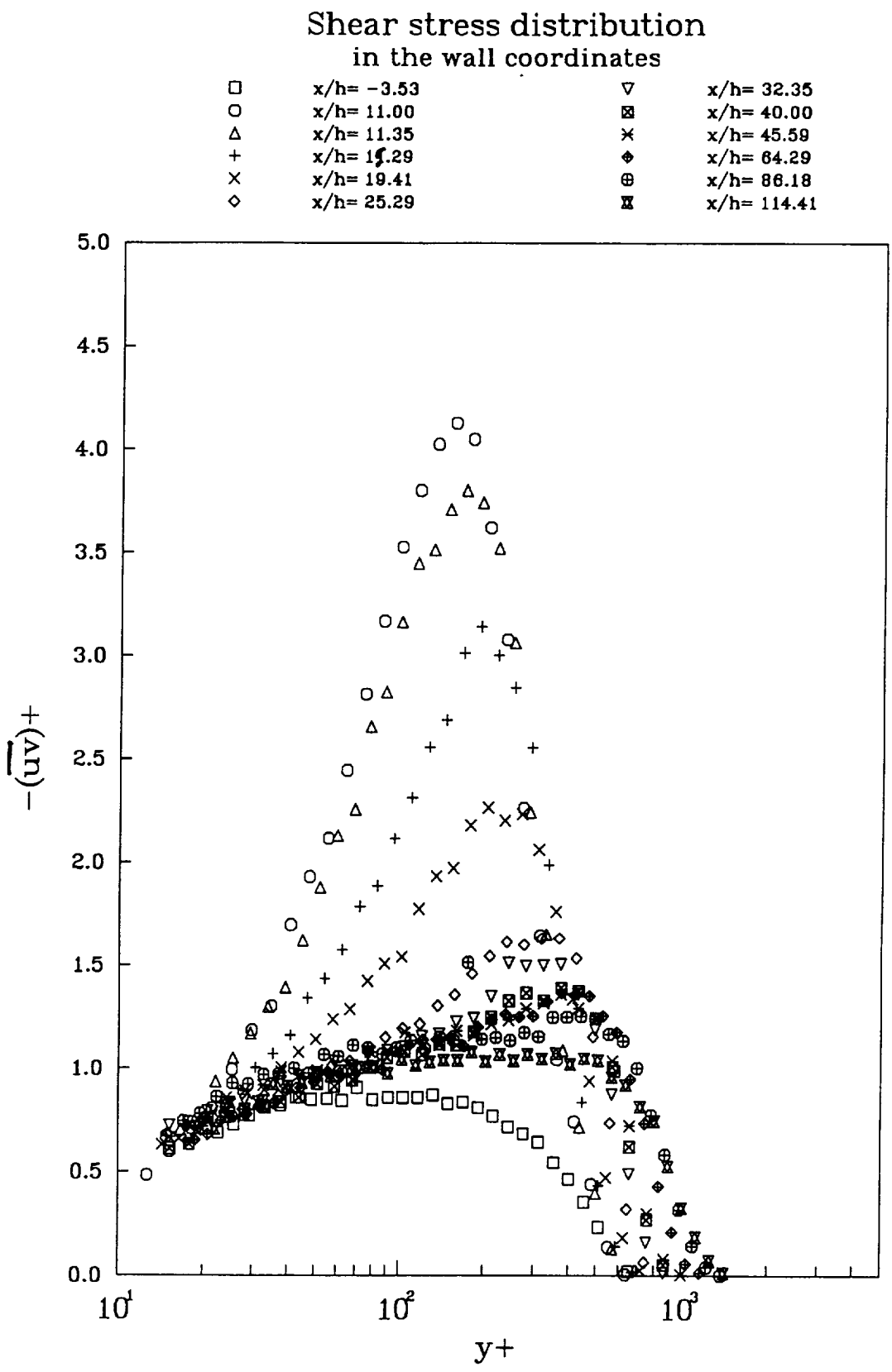
Shear stress distribution
in the wall coordinates
x/h= -3.53
x/h= 11.00
x/h= 11.35
x/h= 15.29
x/h= 19.41
x/h= 25.29
x/h= 32.35
x/h= 40.00
x/h= 45.59
x/h= 64.29
x/h= 86.18
x/h= 114.41
5.0
4.5
4.0
3.5
3.0
2.5
2.0
1.5
1.0
0.5
0.0
$-\overline{(uv)}^+$
10^1
10^2
10^3
y+

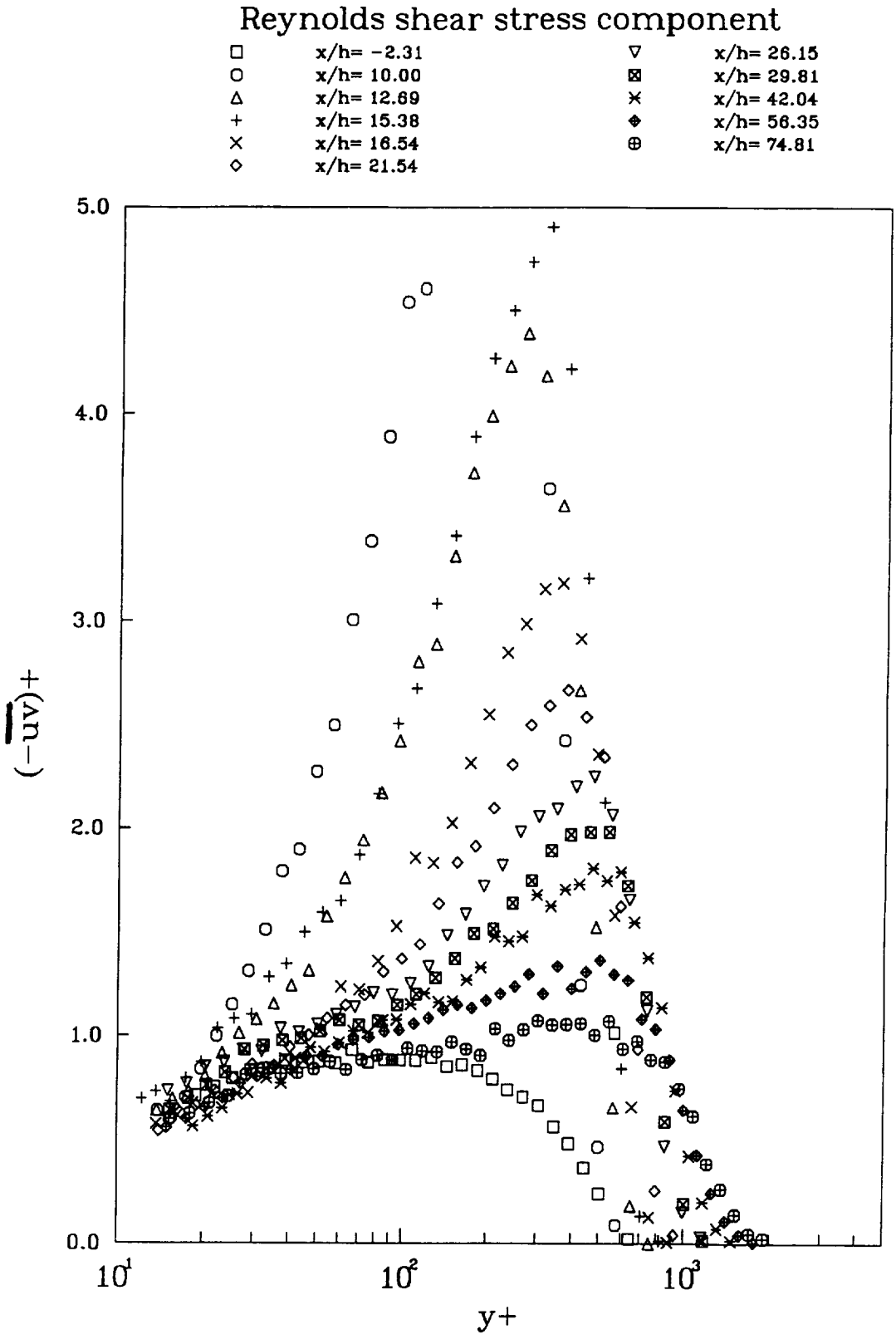
Reynolds shear stress component
x/h= -2.31
x/h= 10.00
x/h= 12.69
x/h= 15.38
x/h= 16.54
x/h= 21.54
x/h= 26.15
x/h= 29.81
x/h= 42.04
x/h= 56.35
x/h= 74.81
5.0
4.0
3.0
2.0
1.0
0.0
$(-\overline{uv})+$
10^1
10^2
10^3
y+

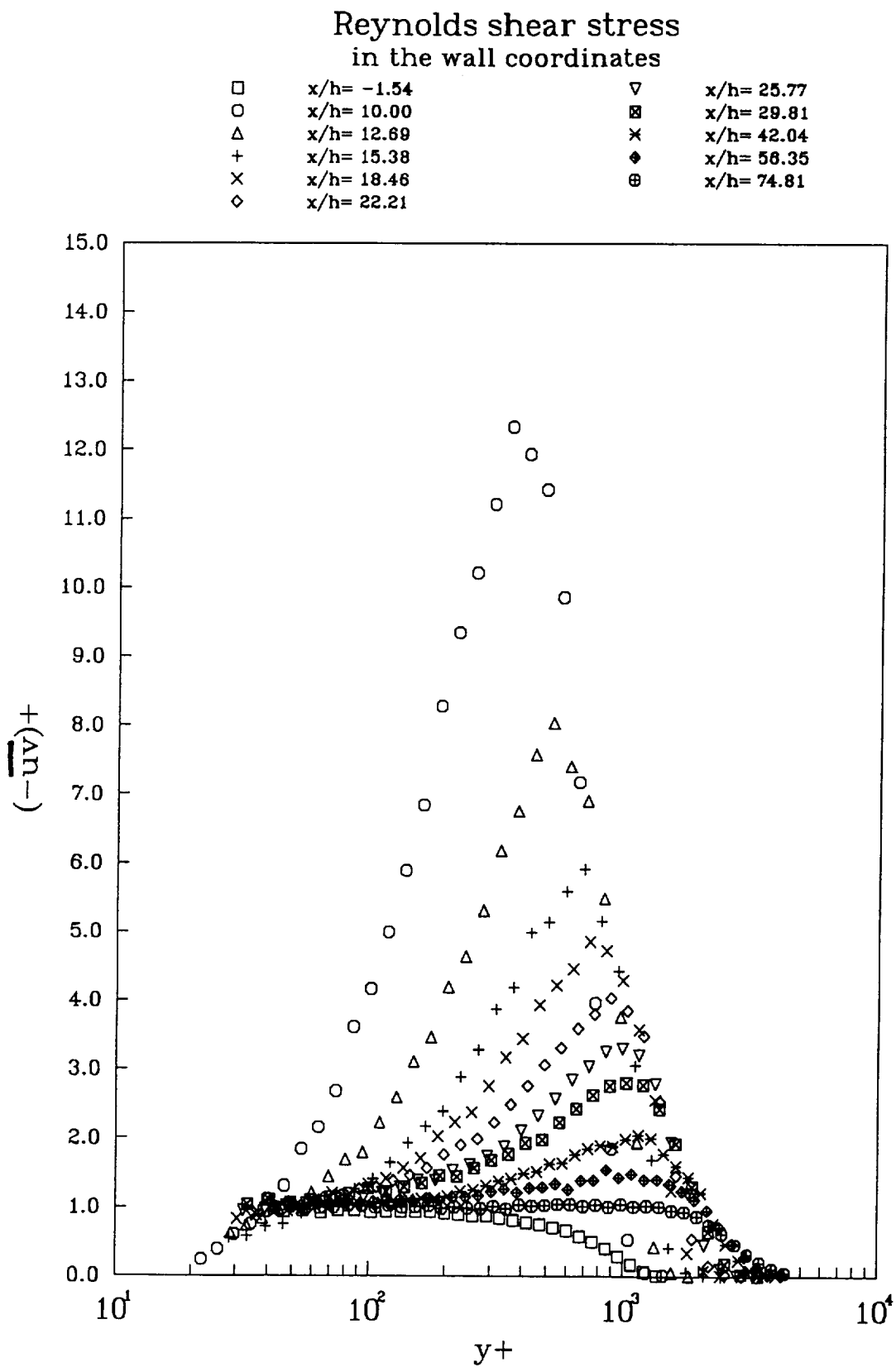
Reynolds shear stress
in the wall coordinates
x/h= -1.54
x/h= 10.00
x/h= 12.69
x/h= 15.38
x/h= 18.46
x/h= 22.21
x/h= 25.77
x/h= 29.81
x/h= 42.04
x/h= 56.35
x/h= 74.81
15.0
14.0
13.0
12.0
11.0
10.0
9.0
8.0
7.0
6.0
5.0
4.0
3.0
2.0
1.0
0.0
10^1
10^2
10^3
10^4
$(-\overline{uv})^+$
y+

Fig 4.19

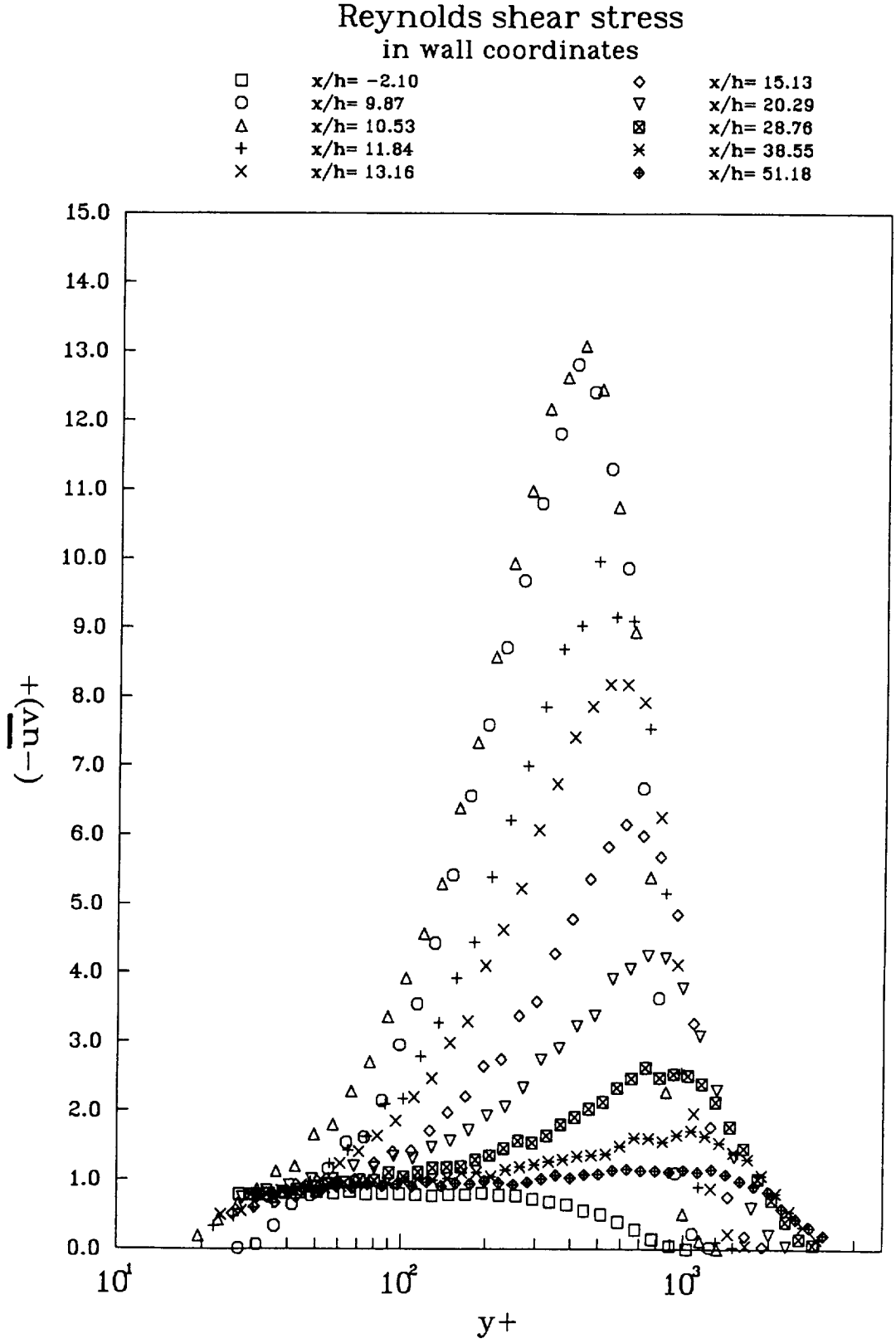
Reynolds shear stress
in wall coordinates
x/h= -2.10
x/h= 9.87
x/h= 10.53
x/h= 11.84
x/h= 13.16
x/h= 15.13
x/h= 20.29
x/h= 28.76
x/h= 38.55
x/h= 51.18
15.0
14.0
13.0
12.0
11.0
10.0
9.0
8.0
7.0
6.0
5.0
4.0
3.0
2.0
1.0
0.0
$(-\overline{uv})+$
10^1
10^2
10^3
y+

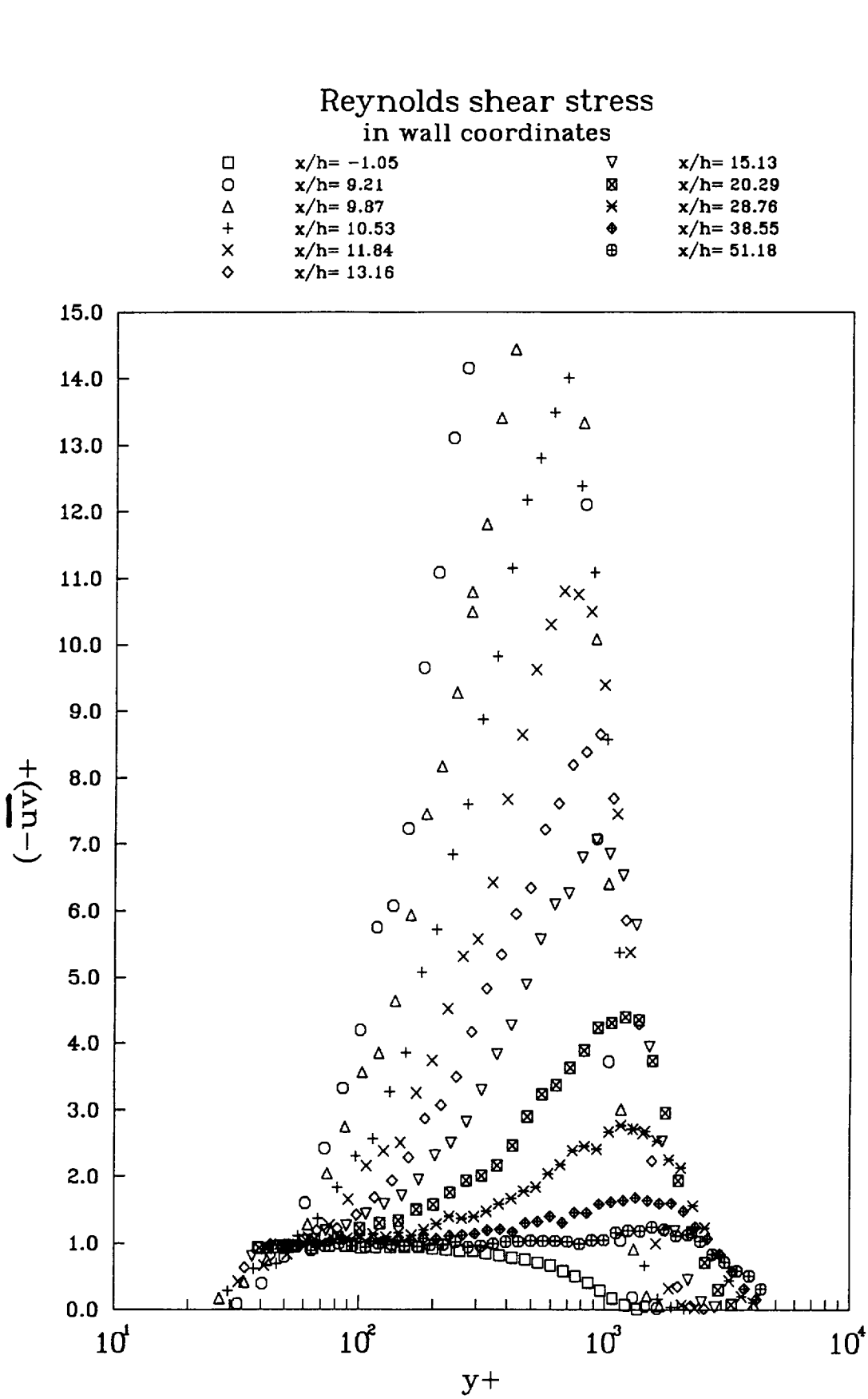
Reynolds shear stress
in wall coordinates
x/h= -1.05
x/h= 9.21
x/h= 9.87
x/h= 10.53
x/h= 11.84
x/h= 13.16
x/h= 15.13
x/h= 20.29
x/h= 28.76
x/h= 38.55
x/h= 51.18
15.0
14.0
13.0
12.0
11.0
10.0
9.0
8.0
7.0
6.0
5.0
4.0
3.0
2.0
1.0
0.0
$(-\overline{uv})+$
10^1
10^2
10^3
10^4
y+

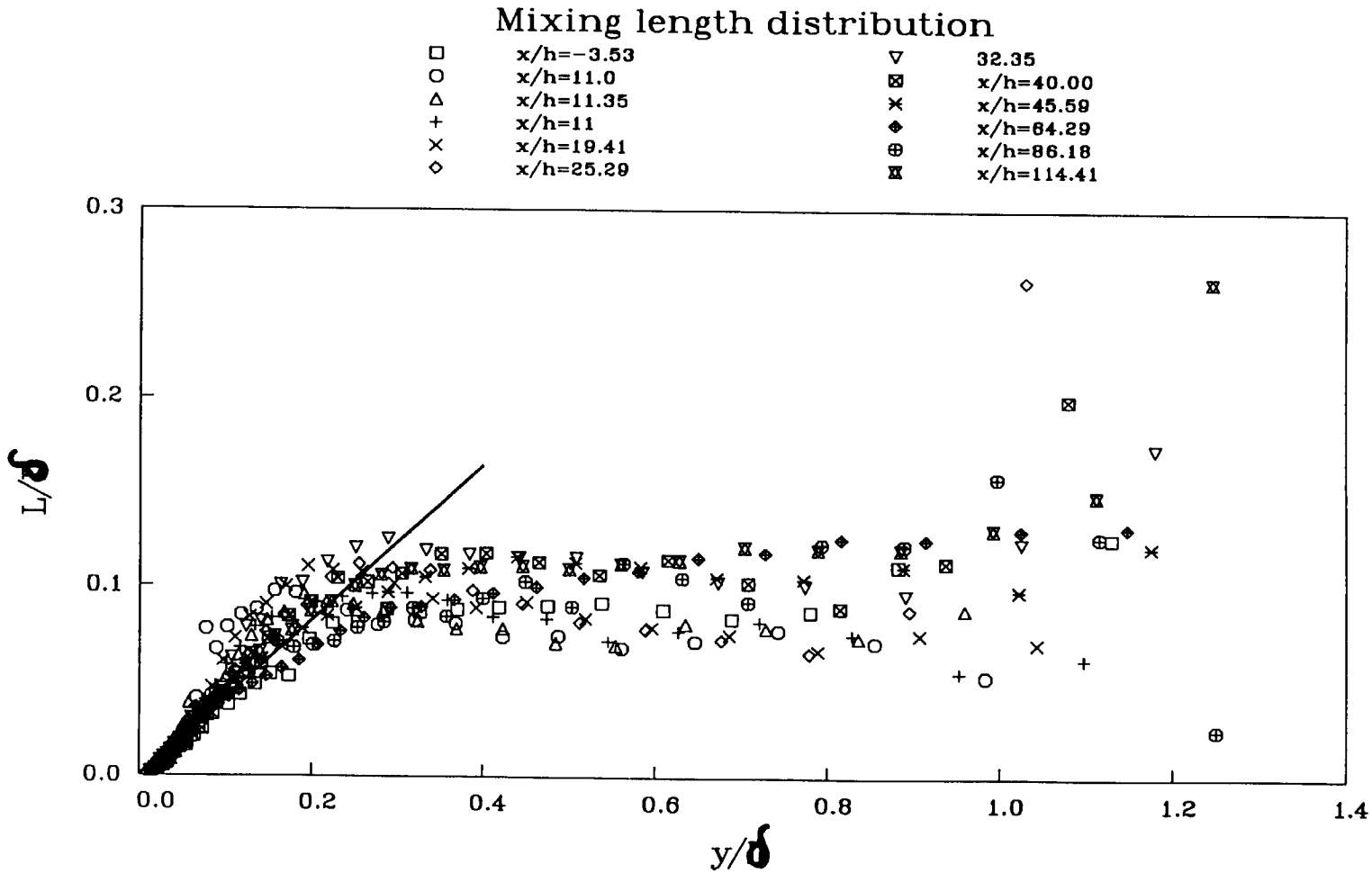
Mixing length distribution
x/h=-3.53
x/h=11.0
x/h=11.35
x/h=11
x/h=19.41
x/h=25.29
32.35
x/h=40.00
x/h=45.59
x/h=64.29
x/h=86.18
x/h=114.41
0.3
0.2
0.1
0.0
L/δ
0.0
0.2
0.4
0.6
0.8
1.0
1.2
1.4
y/δ

Figure 5.19

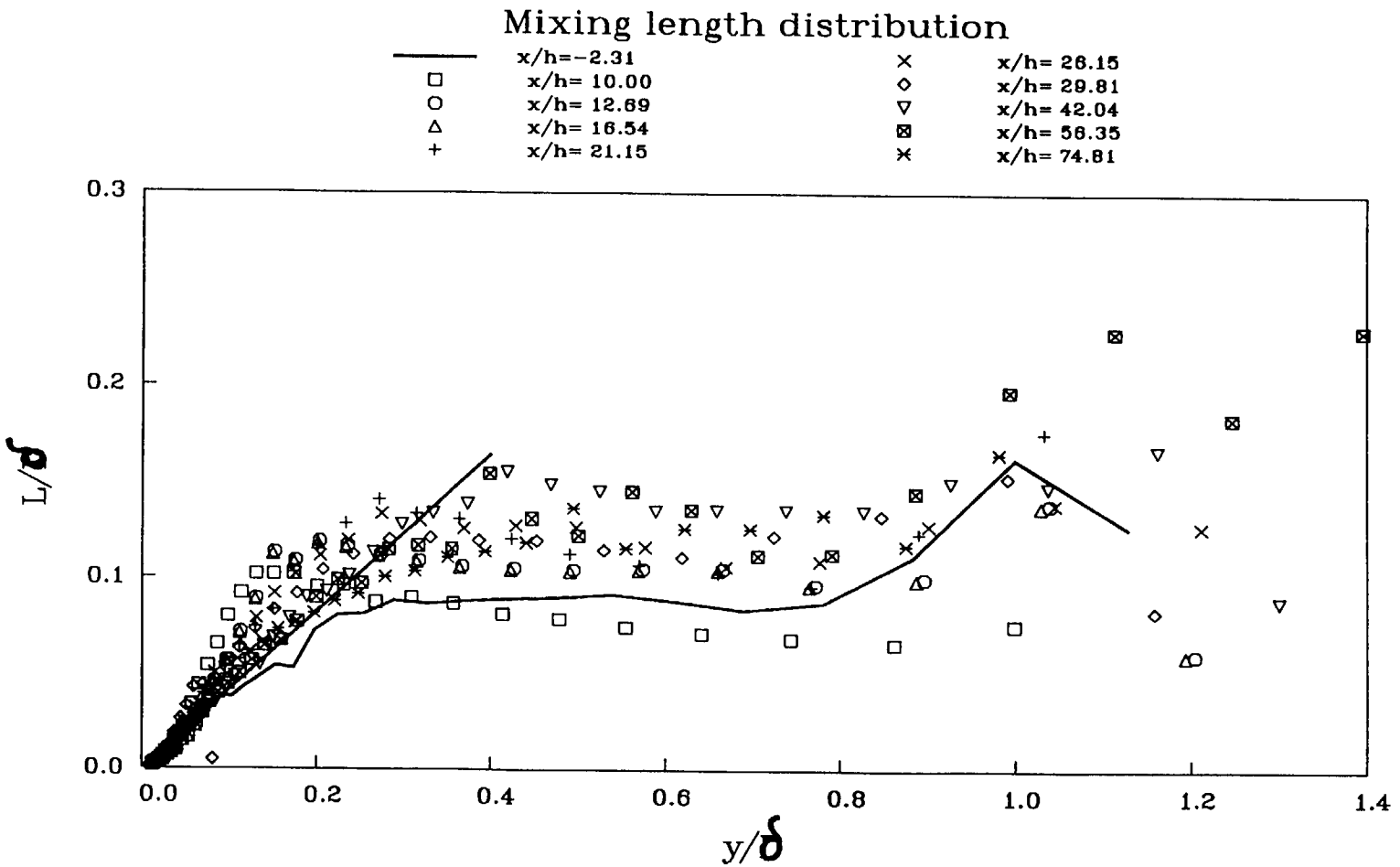
Mixing length distribution
x/h=-2.31
x/h= 10.00
x/h= 12.69
x/h= 16.54
x/h= 21.15
x/h= 26.15
x/h= 29.81
x/h= 42.04
x/h= 56.35
x/h= 74.81
0.3
0.2
0.1
0.0
L/δ
0.0
0.2
0.4
0.6
0.8
1.0
1.2
1.4
y/δ

Figure 5.16)

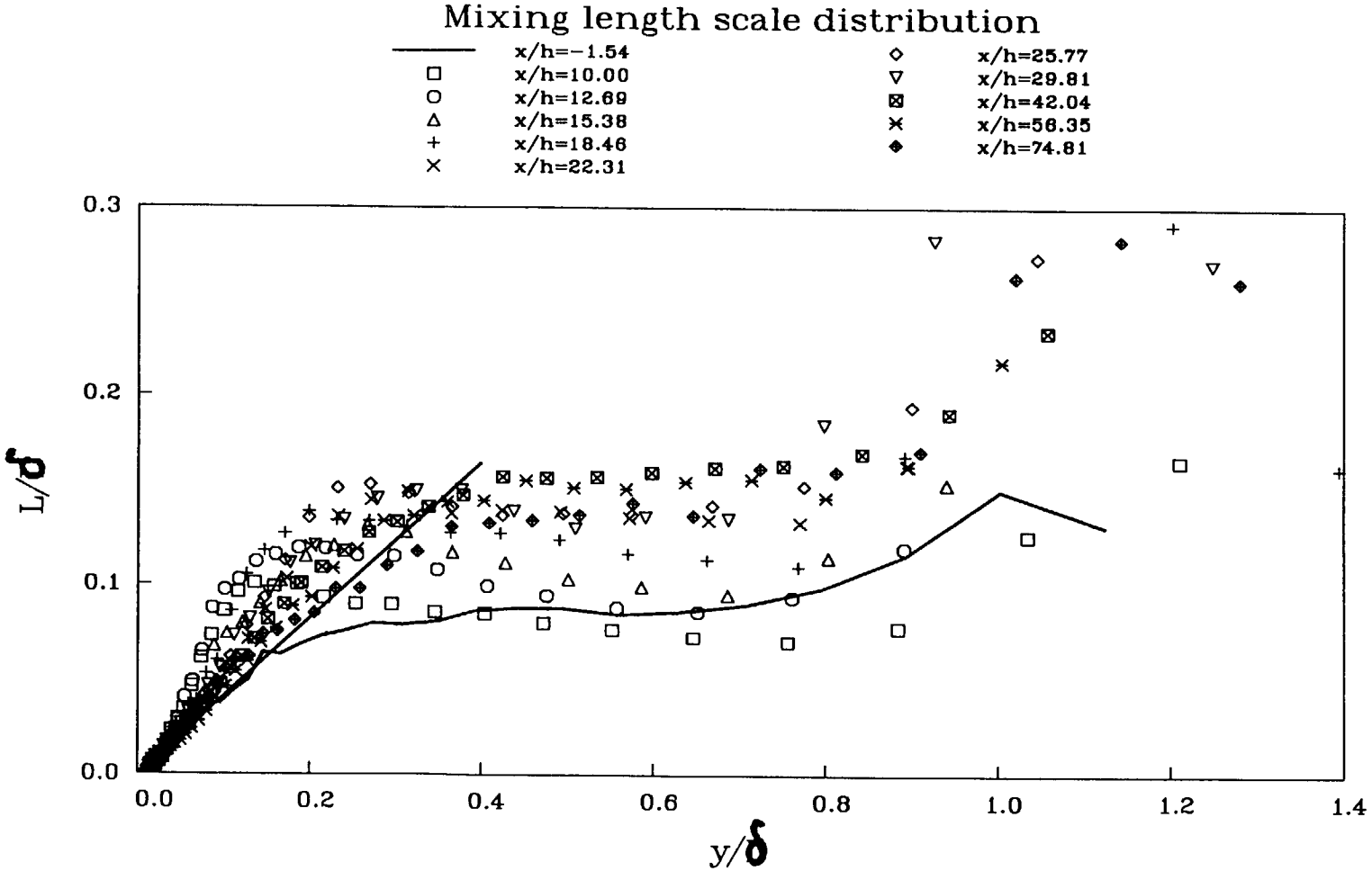
Mixing length scale distribution
x/h=-1.54
x/h=10.00
x/h=12.69
x/h=15.38
x/h=18.46
x/h=22.31
x/h=25.77
x/h=29.81
x/h=42.04
x/h=56.35
x/h=74.81
0.3
0.2
0.1
0.0
L/δ
0.0
0.2
0.4
0.6
0.8
1.0
1.2
1.4
y/δ

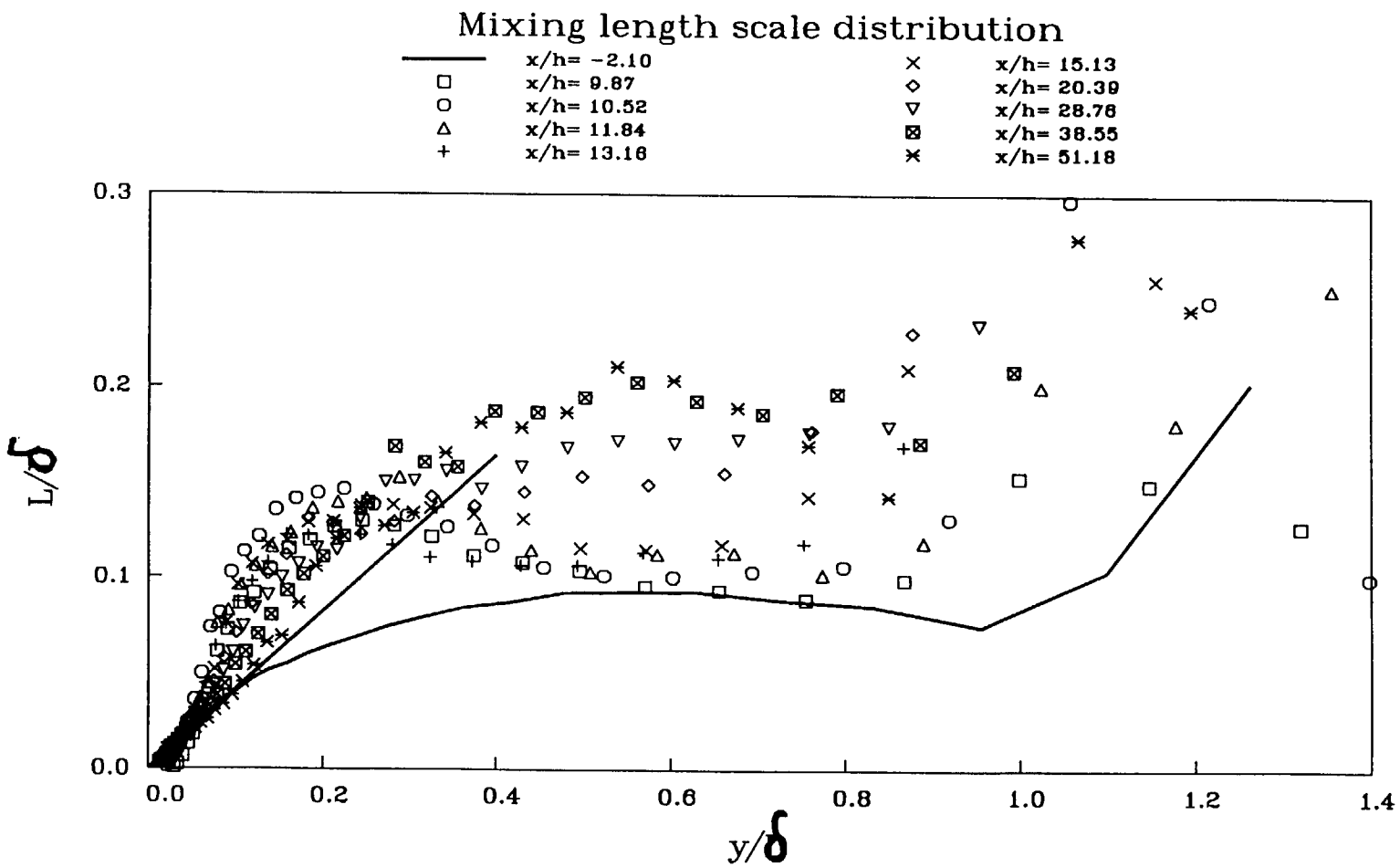
Mixing length scale distribution
x/h= -2.10
x/h= 9.87
x/h= 10.52
x/h= 11.84
x/h= 13.16
x/h= 15.13
x/h= 20.39
x/h= 28.76
x/h= 38.55
x/h= 51.18
0.3
0.2
0.1
0.0
L/δ
0.0
0.2
0.4
0.6
0.8
1.0
1.2
1.4
y/δ

Figure 5.4(a)

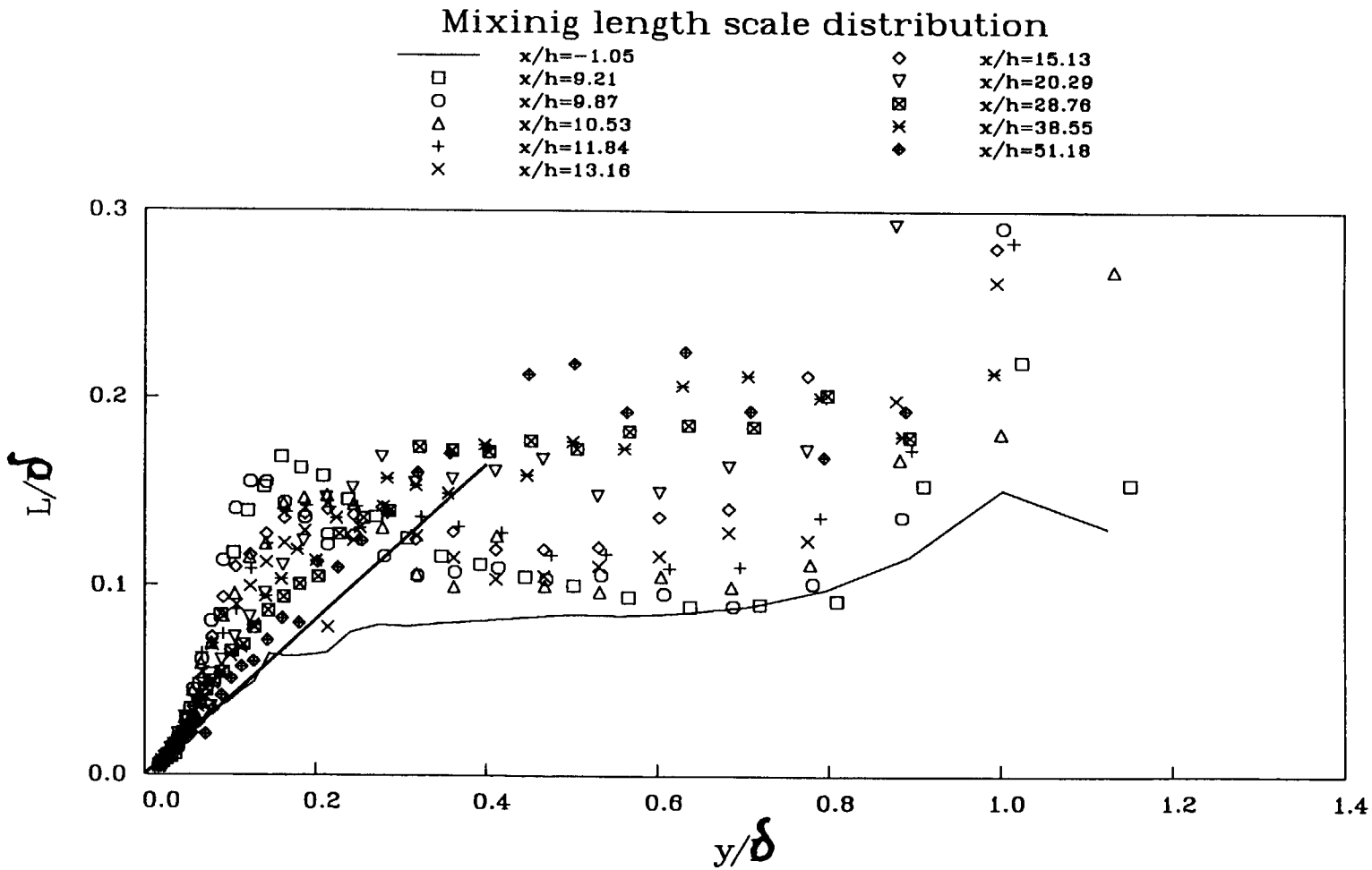
Mixinig length scale distribution
x/h=-1.05
x/h=9.21
x/h=9.87
x/h=10.53
x/h=11.84
x/h=13.16
x/h=15.13
x/h=20.29
x/h=28.76
x/h=38.55
x/h=51.18
0.3
0.2
0.1
0.0
L/δ
0.0
0.2
0.4
0.6
0.8
1.0
1.2
1.4
y/δ

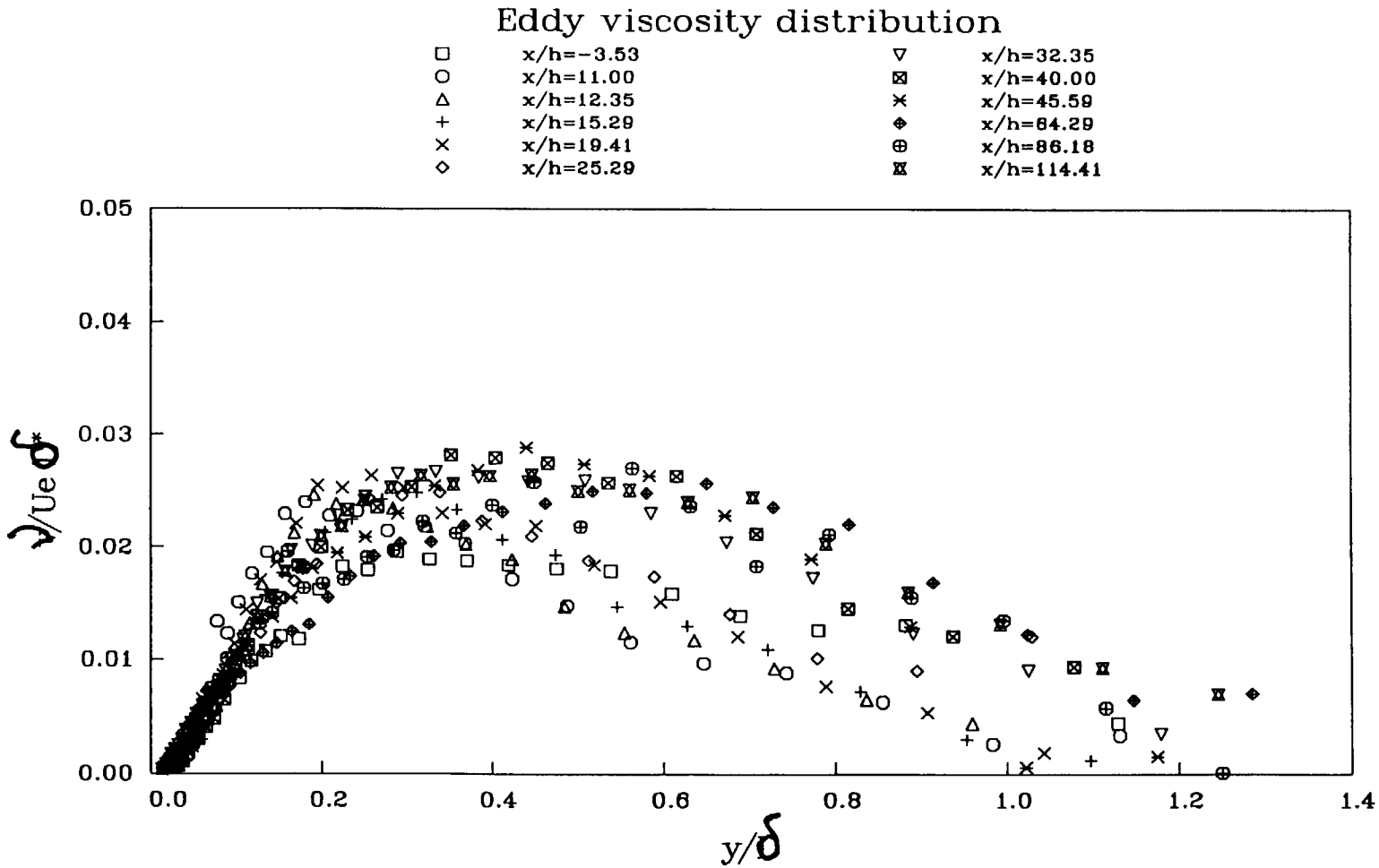
Eddy viscosity distribution
x/h=-3.53
x/h=11.00
x/h=12.35
x/h=15.29
x/h=19.41
x/h=25.29
x/h=32.35
x/h=40.00
x/h=45.59
x/h=64.29
x/h=86.18
x/h=114.41
0.05
0.04
0.03
0.02
0.01
0.00
0.0
0.2
0.4
0.6
0.8
1.0
1.2
1.4
y/δ

Figure 6.(a)

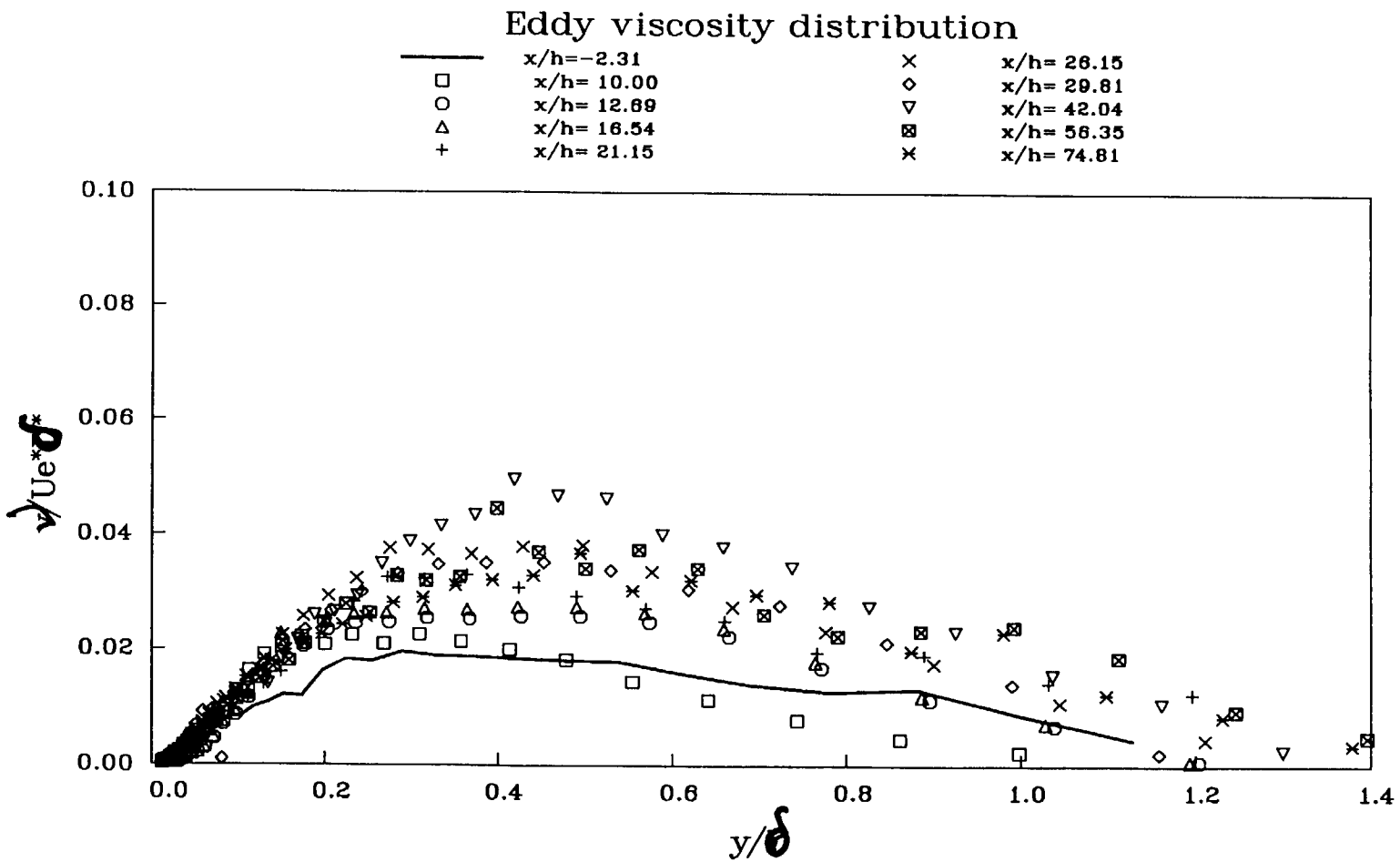
Eddy viscosity distribution
x/h=-2.31
x/h= 10.00
x/h= 12.69
x/h= 16.54
x/h= 21.15
x/h= 26.15
x/h= 29.81
x/h= 42.04
x/h= 56.35
x/h= 74.81
0.10
0.08
0.06
0.04
0.02
0.00
0.0
0.2
0.4
0.6
0.8
1.0
1.2
1.4
ν/Ue*δ*
y/δ

Figure 6.14

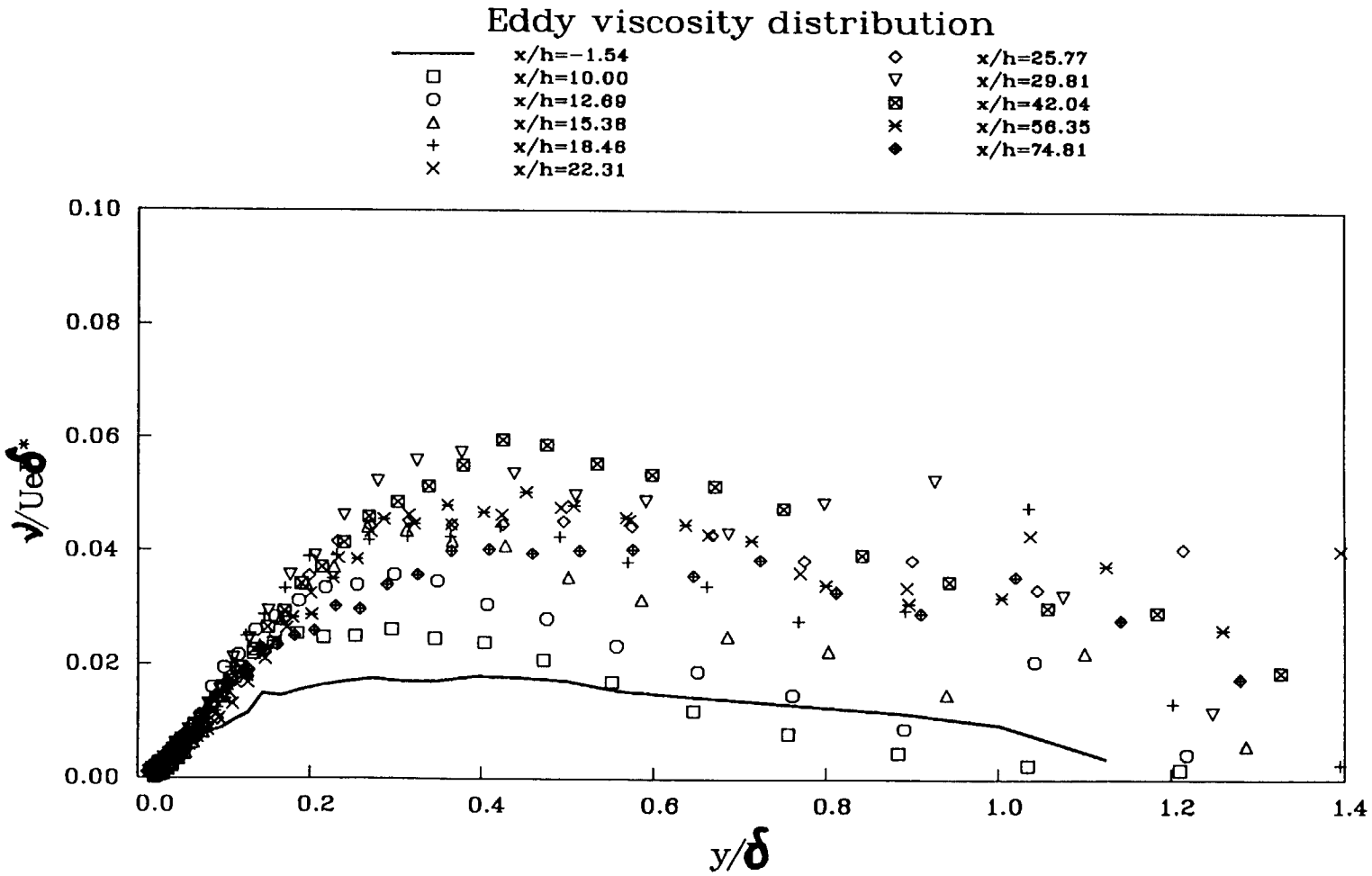
Eddy viscosity distribution
x/h=-1.54
x/h=10.00
x/h=12.69
x/h=15.38
x/h=18.46
x/h=22.31
x/h=25.77
x/h=29.81
x/h=42.04
x/h=56.35
x/h=74.81
0.10
0.08
0.06
0.04
0.02
0.00
0.0
0.2
0.4
0.6
0.8
1.0
1.2
1.4
y/δ

Figure 5.10)

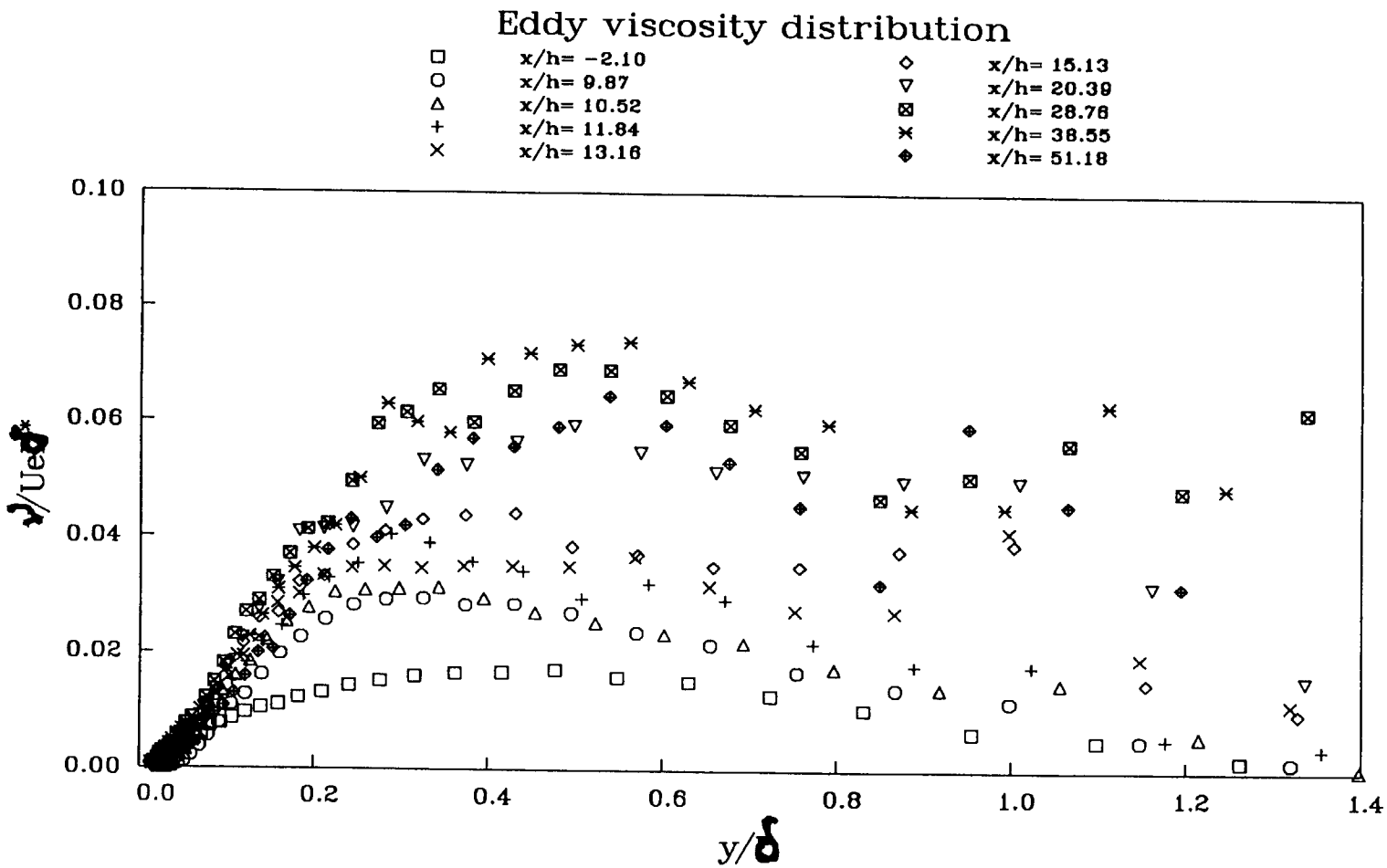
Eddy viscosity distribution
x/h= -2.10
x/h= 9.87
x/h= 10.52
x/h= 11.84
x/h= 13.16
x/h= 15.13
x/h= 20.39
x/h= 28.76
x/h= 38.55
x/h= 51.18
0.10
0.08
0.06
0.04
0.02
0.00
0.0
0.2
0.4
0.6
0.8
1.0
1.2
1.4
y/δ

Figure 6.(d)

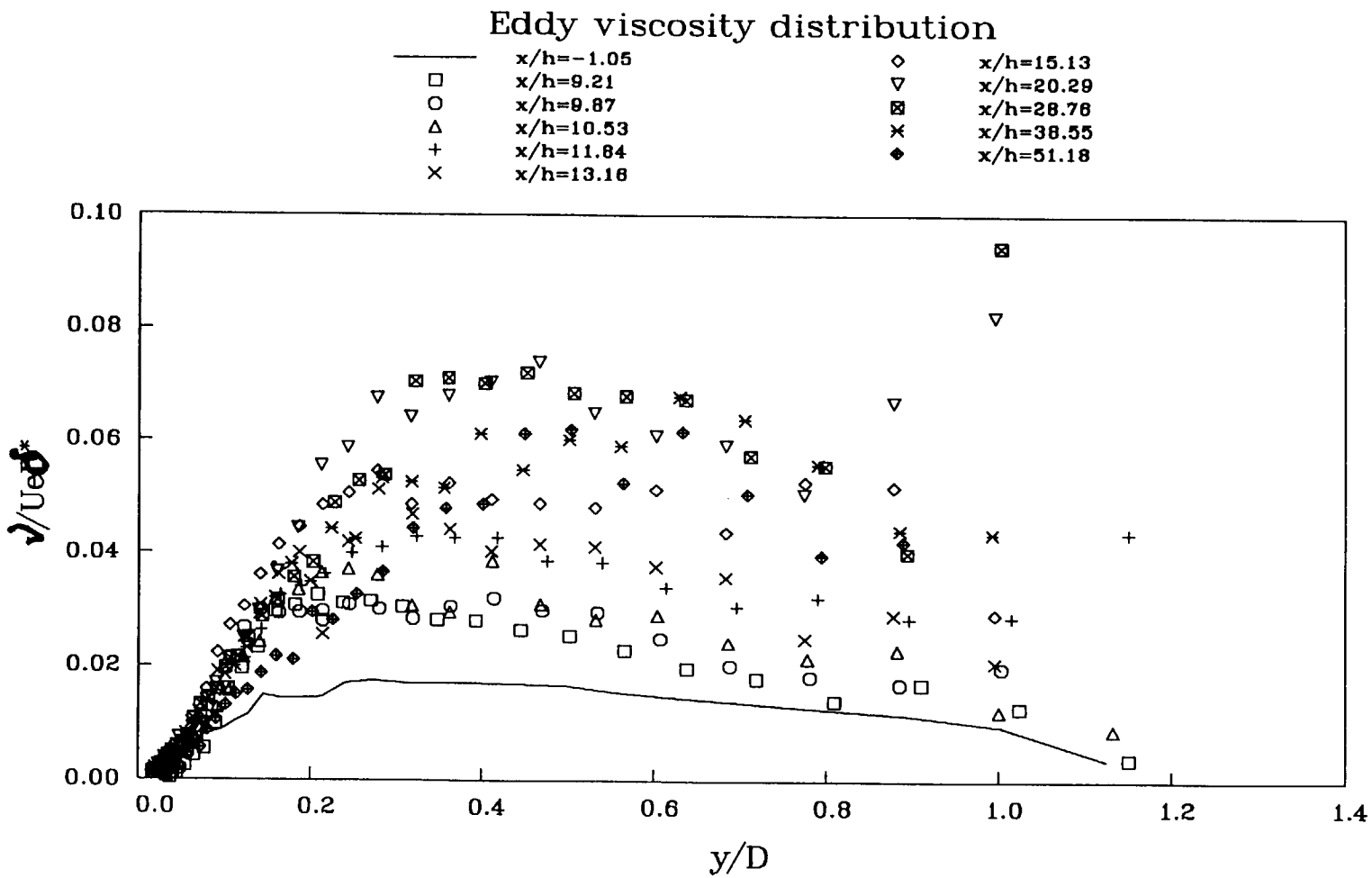
Eddy viscosity distribution
x/h=-1.05
x/h=9.21
x/h=9.87
x/h=10.53
x/h=11.84
x/h=13.16
x/h=15.13
x/h=20.29
x/h=26.76
x/h=36.55
x/h=51.18
0.10
0.08
0.06
0.04
0.02
0.00
0.0
0.2
0.4
0.6
0.8
1.0
1.2
1.4
y/D

Figure 6.(e)